A NUMERICAL METHOD TO MODEL EXCITABLE CELLS

R. W. JOYNER, M. WESTERFIELD, J. W. MOORE, and N. STOCKBRIDGE,
Department of Physiology and Pharmacology, Duke University Medical Center, Durham, North Carolina 27710 U.S.A.

ABSTRACT We have extended a fast, stable, and accurate method for the numerical solution of cable equations to include changes in geometry and membrane properties in order to model a single excitable cell realistically. In addition, by including the provision that the radius may be a function of distance along an axis, we have achieved a general and powerful method for simulating a cell with any number of branched processes, any or all of which may be nonuniform in diameter, and with no restriction on the branching pattern.

INTRODUCTION

Our basic hypothesis is that the cell's electrical behavior results from its morphology as well as its membrane properties. Therefore, the essential information needed to model a cell is:

(*a*) a mathematical model of the membrane ionic conductances and equilibrium potentials as functions of voltage and time specified for each segment of the cell; (*b*) specific cytoplasmic resistivity and specific membrane capacitance; (*c*) detailed cellular geometry.

Previously, we developed the use of the method of Crank and Nicholson (1947) for the implicit integration of cable equations describing axons with excitable membranes. We obtained the solution for the propagating action potential as a function of time and distance (Moore et al., 1975). In this paper, the method is extended to simulate propagation in excitable cells with a wide range and complexity of morphologies.[1]

We assume that all electrical activity of the cell is produced by conductance changes in the cell membrane, and that a small segment of the cell membrane may be represented by a parallel combination of a capacitor and a set of specific ionic conductances in series with specific ionic equilibrium potentials. Our method is general and flexible, allowing the membrane model (the set of equations representing the conductances as functions of voltage and time) to differ for different segments throughout the cell. This

---

Dr. Joyner's present address is: Department of Physiology and Biophysics, University of Iowa, Iowa City, Iowa 52240.

[1]The only geometric restriction is that the cell soma and all branches of cell processes (axons and dendrites) must be surfaces of revolution. That is, the soma and each of the branches must have a structure defined by a radius about some central axis. We are not aware of any cell morphology that this restriction would eliminate from treatment.

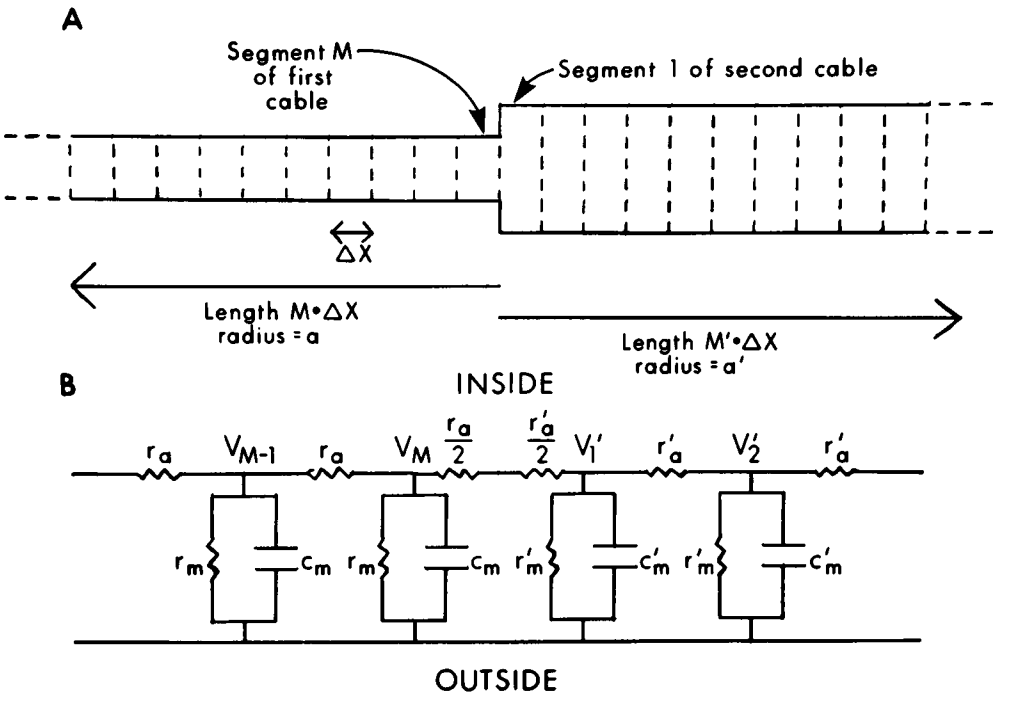

FIGURE 1 Diagram of an axon with an abrupt change of diameter modeled by two attached cables.

makes possible the inclusion of not only electrically excitable but also passive, synaptic, pacemaker, or other desired membrane properties. Although extracellular fields and ionic accumulations can be included in some special cases, we ignore them in this paper.

NUMERICAL METHODS

The methods used to simulate the propagation of action potentials in a cell with branching axons and dendrites are an extension of the Crank-Nicholson (CN) form of implicit solution of the cable equations for a single homogeneous axon (Crank and Nicholson, 1947; Lieberman et al., 1973; Kootsey, 1975; Moore et al., 1975). Because the uniform cable treatment is a building block for the extensions, we include a brief summary of this approach. The basic cable equations are easily derived from the representation of the homogeneous part of the axon, shown in Fig. 1 A as a series of passive isopotential segments of length Δx (cm). The equivalent electrical circuit for its representation as a cable is shown in Fig. 1 B. Each segment is represented by a membrane resistance and capacitance per unit length in parallel. Adjacent segments are coupled by the axoplasmic resistance per unit length r_a. These parameters are derived from the specific membrane resistivity (R_m, ohm·cm^2), specific membrane capacitance (C_m, F/cm^2), the specific axoplasmic resistivity (R_a, ohm·cm) and the axon radius (a, cm) by these relations:

$$r_a = R_a/(\pi a^2) \qquad \text{ohm/cm} \qquad (1a)$$

$$r_m = R_m/(2\pi a) \qquad \text{ohm}\cdot\text{cm} \tag{1b}$$

$$c_m = C_m\cdot(2\pi a) \qquad \text{F/cm} \tag{1c}$$

Replacement of the passive elements by models of excitable membranes (e.g. equations of Hodgkin and Huxley, 1952) allows simulation of action potential propagation in a homogeneous axon by solving, for each time step, the set of CN equations (Moore et al., 1975):

$$-KV_{j-1}^{t+1} + 2(1 + K)V_j^{t+1} - KV_{j+1}^{t+1} = 2(1 - K)V_j^t + K(V_{j+1} + V_{j-1}^t) - \frac{2\Delta t}{c_m} i_j^t \tag{2}$$

where V_j^t is the membrane potential (mV) of segment j at time t, i_j^t is the noncapacitive membrane current (mA/cm) and

$$K = \frac{\Delta t}{r_a c_m (\Delta x)^2}.$$

Or, in a more general form,

$$a_j V_{j-1}^{t+1} + d_j V_j^{t+1} + b_j V_{j+1}^{t+1} = c_j, \tag{3}$$

where

$$a_j = b_j = -K, d_j = 2(1 + K),$$

and

$$c_j = 2(1 - K)V_j^t + K(V_{j+1}^t + V_{j-1}^t) - (2\Delta t/c_m)i_j^t.$$

For an axon consisting of M segments (and length $= M\cdot\Delta x$), we can write down M equations of this form, including M unknowns (V_j^{t+1} for $j = 1, 2, \ldots. M$). The terms a_j, b_j, and d_j are constants, and all of the parameters of c_j are assumed to be known at time t. The boundary conditions at the ends are conveniently included by the addition of virtual (pseudo) segments at each end as follows:

Case 1: grounded ends. In this case, $V_0^t = V_0^{t+1} = 0$ and $V_{M+1}^t = V_{M+1}^{t+1} = 0$ and the general form is the same except that $d_1 = 2(1 + K) = d_M, b_1 = a_M = -K, b_M = a_1 = 0$,

$$c_1 = 2(1 - K)V_1^t + KV_2^t - (2\Delta t/c_m)i_1^t$$

and

$$c_M = 2(1 - K)V_M^t + KV_{M-1}^t - (2\Delta t/c_m)i_M^t.$$

Case 2: sealed ends, or no longitudinal current flow at the ends. In this case we define $V_0^t = V_1^t$; $V_0^{t+1} = V_1^{t+1}$ and $V_{M+1}^t = V_M^t$; $V_{M+1}^{t+1} = V_M^{t+1}$, and the parameters become $d_1 = d_M = 2 + K, b_1 = a_M = -K, b_M = a_1 = 0$,

$$c_1 = (2 - K)V_1^t + KV_2^t - (2\Delta t/c_m)i_1^t$$

and

$$c_M = (2 - K)V_M^t + KV_{M-1}^t - (2\Delta t/c_m)i_M^t.$$

Now let us consider the arrangement in which one end of a uniform cable is connected to one or more additional cables. This situation could represent a model of an axon and a cell body, a dendritic tree, or, in the case of the specific interest here, a branching axon. Taking the simplest case, consider a single cable such that over a length $M \cdot \Delta x$ it has a radius a, and over a length $M' \cdot \Delta x$ it has a radius a' as shown in Fig. 1. Note that the parameters r_m, c_m and r_a are functions of the radius as given in Eqs. 1 *a–c*.

We can preserve the power and form of the CN method to solve the voltage distributions in each cable if we can approximate the boundary conditions for the junction of the two cables. We introduce the term "virtual" ends to indicate the contributions of each cable to the other at the junction.

For each cable we define the virtual voltages V_I and V_F as the equivalent voltages in the segments abutting its initial and final segments if the axon diameters were the same. The values of V_I and V_F are determined from the equality of the longitudinal current flow in the case of the virtual and real junctions. For example, if we assume that the left end of the axon shown in Fig. 1 A is a sealed end (case 2), then $V_I = V_1$. We derive V_F from

$$\frac{V_M - V_F}{r_a} = \frac{V_M - V_1'}{r_a/2 + r_a'/2},$$

therefore,

$$V_F = V_M - \frac{2r_a}{r_a + r_a'}(V_M - V_1'). \tag{4}$$

If we now write the general form of the CN equation for segment M to include the virtual voltage V_F, we get

$$-KV_{M-1}^{t+1} + 2(1 + K)V_M^{t+1} - KV_F^{t+1} = 2(1 - K)V_M^t + K(V_{M-1}^t + V_F^t) - \frac{2\Delta t}{c_m} i_M^t \tag{5}$$

or, rearranged,

$$-KV_{M-1}^{t+1} + 2(1 + K)V_M^{t+1} = 2(1 - K)V_M^t + KV_{M-1}^t + K(V_F^t + V_F^{t+1}) - \frac{2\Delta t}{c_m} i_M^t, \tag{6}$$

and, for segment 1, we get

$$2(1 + K)V^{t+1} - KV^{t+1} = 2(1 - K)V_1^t + KV_2^t + K(V_I^t + V_I^{t+1}) - \frac{2\Delta t}{c_m} i_1^t. \tag{7}$$

Now, to preserve the CN form at the boundaries, for each time step we must compute V_F^t, V_F^{t+1}, V_I^t, and V_I^{t+1}. However, because V_F^{t+1} is a function of V_M and V_1' at time $t + 1$, we must approximate the value of $V_F^t + V_F^{t+1}$, and of $V_I^t + V_I^{t+1}$. We have simply approximated $V_F^t + V_F^{t+1}$ by $2V_F^t$. The error of this approximation leads to a small degree of instability of the solution at the junctional region of the two cables.[2] We have found that this instability

[2]The method used to patch the ends together is an explicit one. Explicit methods become unstable if the $\Delta t/\Delta x^2$ ratio exceeds a certain value; see, for example, Moore et al., 1975.

can be attenuated strongly by alternating the order of solution for the two cables. At one time step the solution for the first cable leads the solution for the second cable and for the next time step the solution for the first cable lags behind the solution for the second cable. This method of alternating the order of solution for the two regions effectively removed the instability at the junctional region. There remains a small oscillation in the solution at the junctional region. The amplitude of the oscillation can be controlled by the choice of the time step for a given value of Δx. When the Δx used was as large as the cell diameter, we found that the oscillations were < 1 mV in amplitude for a Δt of 10 μs or less.

Summarizing, the solution is obtained by the following progression. At time t we (a) compute $V_J = V_1'$,

$$V_F = V_M' - \frac{2r_a}{r_a + r_a'}(V_M' - V_1''),$$

approximate $V_J^t + V_J^{t+1}$ by $2V_J$ and $V_F^t + V_F^{t+1}$ by $2V_F$, (b) integrate all voltages of the first cable by solving the set of CN equations for one time step; this gives us V_M^{t+1} to use in finding V_J'. (c) For the second cable compute

$$V_J' = V_1'' - \frac{2r_a'}{r_a + r_a'}(V_1'' - V_M^{t+1}),$$

$V_F' = V_M'$, and approximate $V_J'^t + V_J'^{t+1}$ by $2V_J'$ and $V_F'^t + F_f'^{t+1}$ by $2V_F'$. (d) Integrate all voltages of the second cable by solving the second set of CN equations for one time step.

At time $t + 1$ we reverse the order of solution so that, for the second cable, we use

$$V_J' = V_J'^{t+1} - \frac{2r_a'}{r_a + r_a'}(V_1'^{t+1} - V_M^{t+1}),$$

approximate $V_J'^{t+1} + V_J'^{t+2}$ by $2V_J'$, and integrate the second cable one time step. Then for the first cable, we compute

$$V_F = V_M^{t+1} - \frac{2r_a}{r_a + r_a'}(V_M^{t+1} - V_1''^{t+2}),$$

approximate $V_F^{t+1} + V_F^{t+2}$ by $2V_F$, and integrate the first cable one time step.

Boundary Conditions for a Branching Axon

For the branching axon shown in Fig. 2 we can use the same method of virtual ends to solve for $V(t)$ for each segment of the three cables modeling the branching axon. For the first cable (radius = a), we use $V_J = V_1$ for a sealed end (or $V_J = 0$ for a grounded end), and we derive V_F from

$$\frac{V_M - V_F}{r_a} = \frac{V_M - V_1'}{r_{a/2} + R_{a/2}'} + \frac{V_M - V_1''}{r_{a/2} + r_{a/2}''}$$

or, rearranged to give the voltage at the virtual end,

$$V_F = V_M - \left(\frac{2r_a}{r_a + r_a'}\right)(V_M - V_1') - \left(\frac{2r_a}{r_a + r_a''}\right)(V_M - V_1''). \tag{8}$$

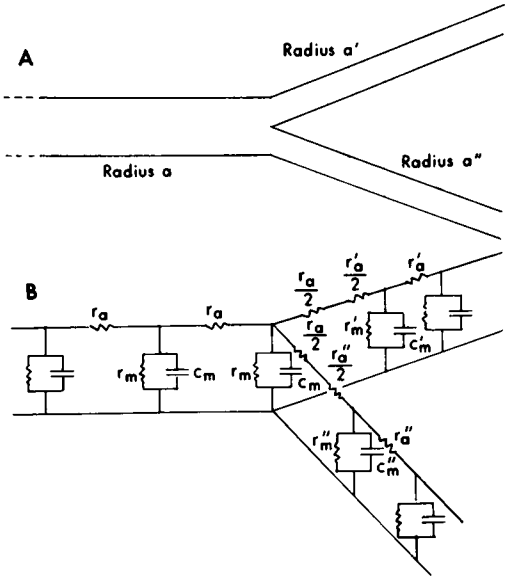

FIGURE 2 Diagram of a branching axon modeled by three cables attached at the branch point.

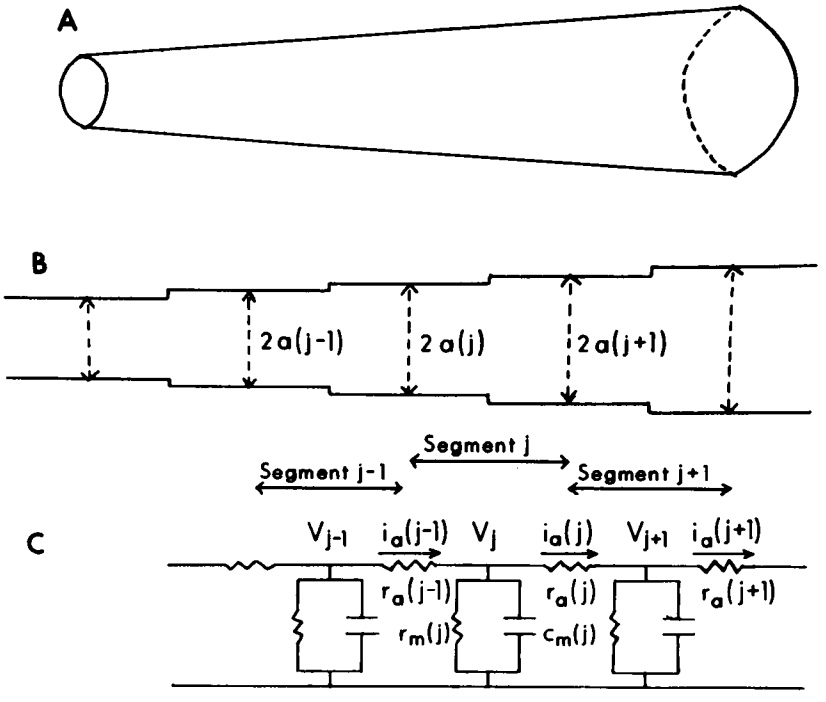

FIGURE 3 Diagram of a cell with a continuously variable radius modeled by a cable whose elements represent stepwise variations in radius.

For the second cable (radius = a'), we use

$$V_I' = V_1' - \frac{2r_a'}{r_a' + r_a}(V_1' - V_M),$$

and for the third cable (radius = a''), we use $V_I'' = V_1'' - [2r_a''/(r_a + r_a'')](V_1'' - V_M)$.

As before, we must approximate the values for $V_I^t + V_I^{t+1}$ and $V_F^t + V_F^{t+1}$. Note that the order of the CN solution for cables two and three (radii = a' and a'') does not matter at all because their boundary conditions do not interact for any given time step. Although each branch must be represented by a one-dimensional cable, the branches can be of any length and any radius, and any number of branches may come from a single point. It should be clear that this method can be extended to any branching network of fibers. Furthermore, the method can also handle variable radii along any or all branches as is shown in the next section.

Solution for Axons of Varying Radius

Simulations of propagation of action potentials along a fiber of variable radius has been previously reported for analytical treatment of special cases (Goldstein and Rall, 1974) and an iterative numerical integration method (Cooley and Dodge, 1966; Parnas et al., 1976). The Crank-Nicholson method can be extended to include an axon with variable radius. This is illustrated in Fig. 3, where A shows a portion of an axon with continuously varying radius and B shows the approximation of this geometry by a series of straight segments of length Δx. Note that the set of radii $a(j)$ are defined so that $a(j)$ is the radius for the first half of segment j, and $a(j + 1)$ is the radius of the second half of segment j. With this geometry we now redefine our basic parameters as

$$r_m(j) = \frac{R_m}{\pi[a(j) + a(j + 1)]} \tag{9a}$$

$$c_m(j) = C_m \cdot [a(j) + a(j + 1)] \cdot \pi \tag{9b}$$

$$r_a(j) = \frac{R_a}{\pi[a(j + 1)]^2}, \tag{9c}$$

where $r_m(j)$, $c_m(j)$, and $r_a(j)$ are the components of the equivalent circuit in Fig. 3 C.

To derive a form of the CN equations applicable to this case, we first note that

$$i_a^t(j) = \frac{V_j^t - V_{j+1}^t}{\Delta x \cdot r_a(j)} \tag{10}$$

and

$$I_j^t = \frac{i_a^t(j - 1) - i_a^t(j)}{\Delta x} = c_m(j)\frac{\partial V_j}{\partial t} + i_j^t, \tag{11}$$

where $i_a^t(j)$ is the axial current (mA) at time t at segment j and I_j^t is the total membrane current at segment j at time t. To convert this to a form that can be numerically integrated, we write the difference form, using the average value of i_a between time t and time $t + 1$:

$$\frac{i_a^t(j - 1) - i_a^t(j) + i_a^{t+1}(j - 1) - i_a^{t+1}(j)}{2\Delta x} = \frac{c_m(j)}{\Delta t}[V_j^{t+1} - V_j^t] + i_j^t. \tag{12}$$

Now, multiplying through by $\left(\frac{-2\Delta t}{c_m(j)}\right)$ and substituting for i_a we get

$$\frac{\Delta t}{\Delta x^2 c_m(j)}\left[\frac{V_j^t - V_{j+1}^t}{r_a(j)} - \frac{V_{j-1}^t - V_j^t}{r_a(j-1)} + \frac{V_j^{t+1} - V_{j+1}^{t+1}}{r_a(j)} - \frac{V_{j-1}^{t+1} - V_j^{t+1}}{r_a(j-1)}\right]$$

$$= 2[V_j^t - V_j^{t+1}] - \frac{2\Delta t}{c_m(j)} i_j^t \qquad (13)$$

or, rearranged,

$$-K_j' V_{j-1}^{t+1} + [2 + K_j + K_j'] V_j^{t+1} - K_j V_{j+1}^{t+1} =$$

$$K_j' V_{j-1}^t + [2 - K_j - K_j'] V_j^t + K_j V_{j+1}^t - \frac{2\Delta t}{c_m(j)} i_j^t,$$

where

$$K_j = \Delta t / c_m(j) r_a(j+1) \Delta x^2, \text{ and } K_j' = \Delta t / c_m(j) r_a(j) \Delta x^2.$$

The general form of the CN equations has still been preserved: $a_j V_{j-1}^{t+1} + d_j V_j^{t+1} + b_j V_{j+1}^{t+1} = c_j$ but $a_j = -K_j'$, $b_j = -K_j$, $d_j = 2 + K_j' + K_j$, and

$$c_j = K' V_{j-1}^t + [2 - K_j - K_j'] V_j^t + K_j V_{j+1}^t - \frac{2\Delta t}{c_m} i_j^t.$$

Boundary conditions can now be easily defined as in the homogeneous axon simulation.

Solution for Myelinated Axons

We have also extended the CN method to simulate action potential propagation along myelinated fibers. This was done by making the r_m and c_m for those segments that contain a node different from those segments that are completely myelinated. The constants for myelinated segments are calculated on the assumption that it is composed of a large number of turns of passive membrane. Any of several descriptions for active membranes can be used to describe the nodal area. This extension is presented in detail elsewhere (Moore et al., 1978).

RESULTS

Goldstein and Rall (1974) presented a method for simulating the propagation of action potentials along fibers in which the variation of the radius with length could be described by certain analytical functions. They used a kinetic model for the membrane conductances which produced an action potential similar to a squid giant axon at 26°C. We have used exclusively the equations of Hodgkin and Huxley (1952) as the mathematical model of membrane conductances as functions of voltage and time. This allows us to test our simulations directly by performing experiments on squid giant axons (see Ramón et al., 1975; 1976). Also it allows us to study the effect of temperature in the simulations, because we can change the effective temperature by scaling the rate constants by a value computed from a Q_{10} of 3 and a base temperature of 6.3°C.

Our simulations of action potentials propagating along inhomogeneous axons (those with nonconstant diameter) are similar to those obtained by Khodorov et al., (1969),

Goldstein and Rall (1974), and Parnas et al. (1976). As the action potential approaches a region of increased diameter, the maximum amplitude, V_{max}, the conduction velocity, θ, and the maximum rate of rise, $\dot{V}_{max}$, all decrease. The safety factor for propagation at this region is lowered, and propagation through this region will fail if the ratio of diameter (large/small) is above a critical value. This critical value is lowest for an abrupt increase in diameter, but increases as the transition from the small to large diameter is made more gradual. We also found that the critical value of the diameter ratio was strongly dependent on temperature.

For all of the simulations reported here, we used a Δx of 200 μm, a Δt of 5 μs, and a 100-segment cable (total length $100 \times \Delta x = 2$ cm). The effective temperature was 16.3°C unless otherwise specified. For all of the simulated axons, the point of stimulation is to the left of the region diagrammed in the figures. We have plotted results only for those segments in the central portion of the cable to avoid the changes in V_{max}, $\dot{V}_{max}$, and θ produced by the boundary conditions at the ends. We have used axon diameters appropriate for the squid giant axons, but the results reported here are applicable to smaller axons as well, inasmuch as the effects of a change in radius depend on the diameter ratio and not on the actual values of the diameters.

How an abrupt change in diameter affects θ, V_{max}, and $\dot{V}_{max}$ is shown in Fig. 4 for diameter changes from 100 to 200 μm (A) or to 500 μm (B). We defined the conduction velocity as $\Delta x/\Delta T$, where Δx is the segment length and ΔT is the difference in the times at which the action potential reaches 50 mV in amplitude at adjacent segments. Because the action potential shape changes dramatically near the transition region, this

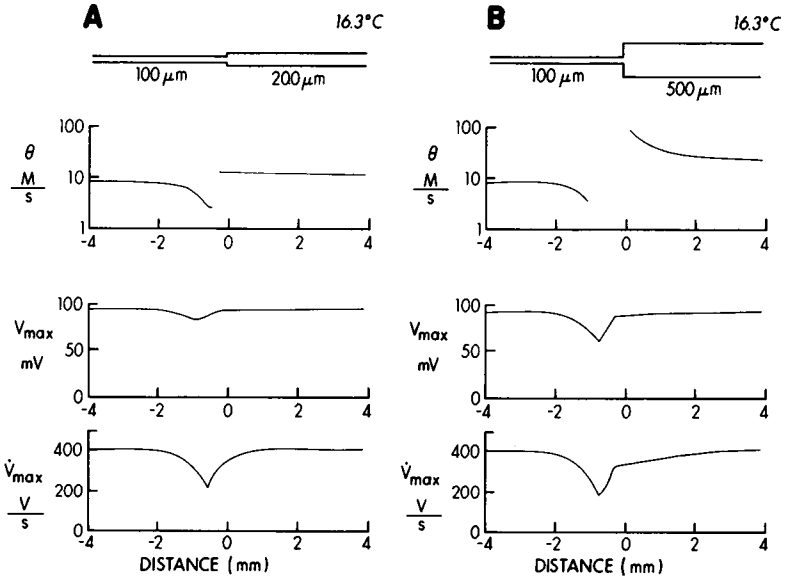

FIGURE 4 Simulation of θ, V_{max}, and $\dot{V}_{max}$ (as functions of distance along the axon) for action potentials propagating along fibers with abrupt diameter increases as diagrammed in the figure.

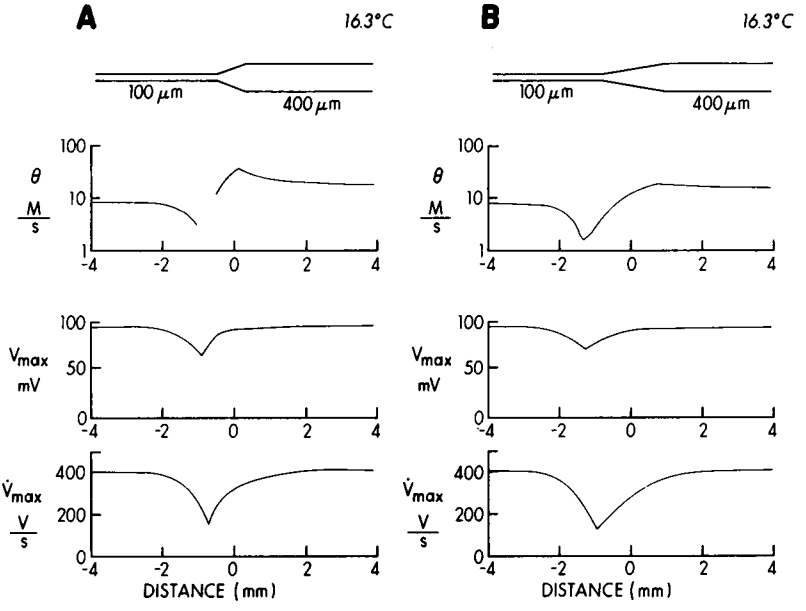

FIGURE 5 Simulation of θ, V_{max}, and $\dot{V}_{max}$ (as functions of distance along the axon) for action potentials propagating along fibers with diameter increases occurring over a length of 600 (A) or 1,800 μm (B) as diagrammed in the figure.

definition of conduction velocity no longer accurately represents the velocity of the traveling impulse. We have simply deleted from the figures those values of θ near the transition region, that were clearly meaningless. The conduction velocity decreases as the action potential approaches the transition region, jumps to a very large value as it enters the region of larger diameter, and settles down to the new high velocity for the larger diameter. Both V_{max} and $\dot{V}_{max}$ decrease as the action potential approaches the transition region, then show a rapid recovery to their normal values as the action potential enters the region of larger diameter. All of these effects become more marked as the diameter ratio is increased.

Because our method allows the diameter to be any function of distance along the fiber, we were able to study also how these variables changed when the transition in diameters was accomplished with a linear increase over a distance L. Fig. 5 shows how θ, V_{max}, and $\dot{V}_{max}$ are affected by a diameter increase occurring over a short distance (A, 600 μm) and over a longer distance (B, 1,800 μm). As might be expected, making the taper more gradual diminishes and distributes the disturbances in all three variables over a larger distance.

If the action potential propagates through a transition from a large to small diameter, changes in θ, V_{max}, and $\dot{V}_{max}$ are different, as shown in Fig. 6. Here, θ, V_{max}, and $\dot{V}_{max}$ all increase as the action potential approaches the transition region, then decrease to steady values in the smaller fiber. These changes are produced by the smaller electrical load seen by the action potential as the transition is approached from

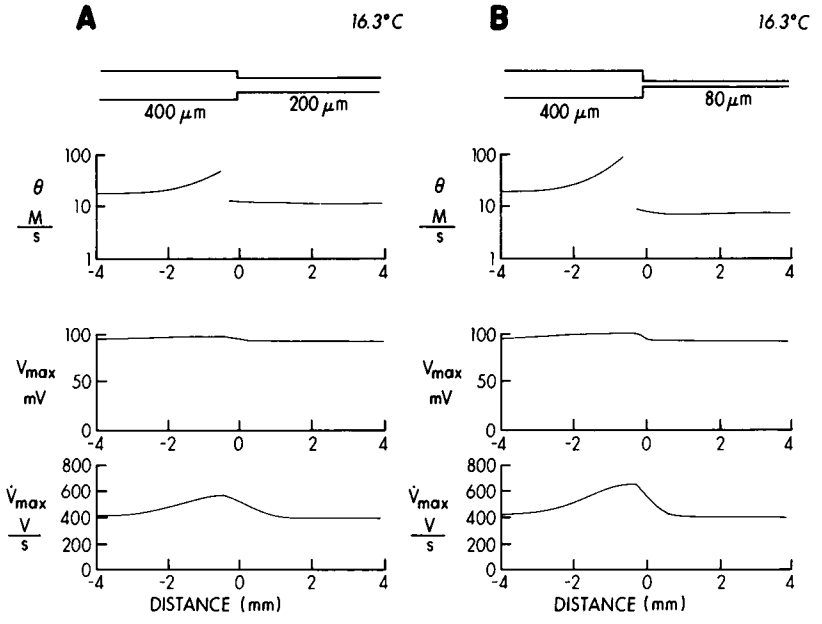

FIGURE 6 Simulation of θ, V_{max}, and $\dot{V}_{max}$ (as functions of distance along the axon) for action potentials propagating in a fiber with abrupt diameter decreases as diagrammed in the figure.

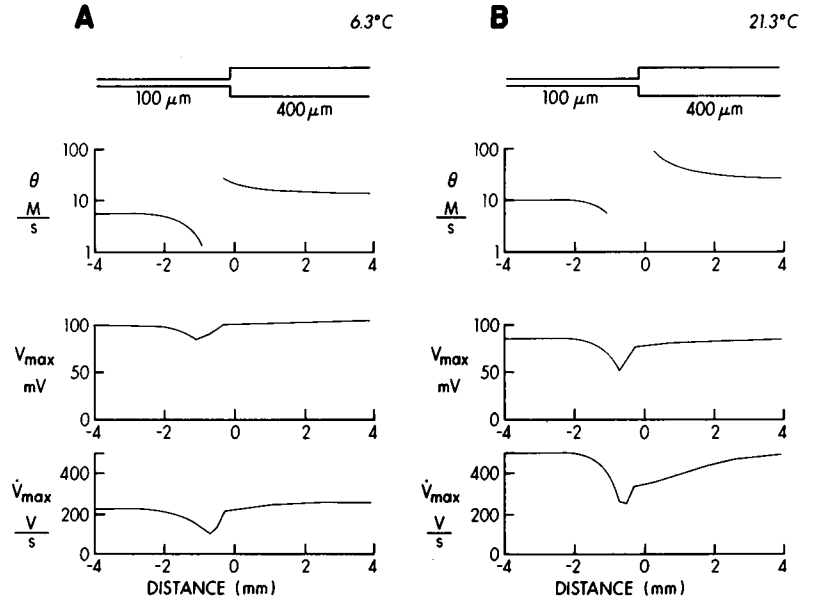

FIGURE 7 Simulation of θ, V_{max}, and V_{max} (as functions of distance along the axon) for action potentials propagating along fibers with abrupt diameter increases as shown in the figure. The effective temperature is 6.3°C (A) or 21.3°C (B).

the larger diameter region. In the limit, as the smaller diameter approaches zero, the situation represents a fiber with a sealed end (see case 2 under Methods). If the diameter decreases gradually, the effects on θ, V_{max}, and $\dot{V}_{max}$ are diminished and distributed along the fiber, similar to the results for a gradual diameter increase.

At higher temperatures, there is a more marked effect of the diameter change on all three variables, θ, V_{max}, and $\dot{V}_{max}$, as can be seen in Fig. 7 for an abrupt diameter increase from 100 to 400 μm at temperatures of 6.3° (A) and 21.3°C (B). Note that the steady values, in the homogeneous regions of the axon, of θ, V_{max}, and $\dot{V}_{max}$ are functions of temperature.

A change in the effective temperature also changes the critical value of the diameter ratio at which propagation of action potentials will fail at the transition region, as shown in Fig. 8. This critical value is rather high at low temperatures, 10-fold at 6°C, but drops to approximately 3.5 at 26°C. The critical ratio seems to be closely correlated with the duration of the Hodgkin-Huxley action potential which changes by about fivefold over this temperature range. Goldstein and Rall (1974) found the same critical ratio (3.5) using a kinetic model for the membrane conductances. Their action potential duration was similar to that computed from the Hodgkin-Huxley equations for 26°C.

Goldstein and Rall (1974) stated that, for a branching axon, there are similar effects on θ, V_{max}, and $\dot{V}_{max}$ if the load ratio of the daughter branches to the parent fiber is greater than unity (expressed here as a geometric ratio):

$$GR = \frac{\Sigma d_j^{3/2}}{d_a^{3/2}},$$

where d_a is the diameter of the parent fiber and the d_j are the diameters of the branches. Although these authors did not present their method or any numerical results for propagation of action potentials along branching fibers, they stated that when GR was greater than unity they found changes in the action potential shape and velocity similar to those found for a single fiber with an abrupt change in radius. They further stated that at a critical GR there was propagation failure and that at some value of GR less than this critical ratio there was retrograde propagation along the stimulated fiber as well as in the branches.

Our method, using the Hodgkin-Huxley equations for the membrane properties and the extended Crank-Nicholson method for the geometric properties of a branching fiber, produces qualitatively similar results, with the additional finding that the effect of a given GR was strongly dependent on temperature. These results, along with experimental confirmation of this effect of temperature on failure at squid axon branch points, are presented in detail elsewhere (Westerfield et al., 1978).

Simulation of action potential propagation near the junction of a small (100 μm) axon and a larger (200 μm) axon is shown in Fig. 9 A. The arrows point to the segments from which the voltages are shown in Fig. 9 B. The effects on the shape of the action potential in the transition region are very similar to those described for the

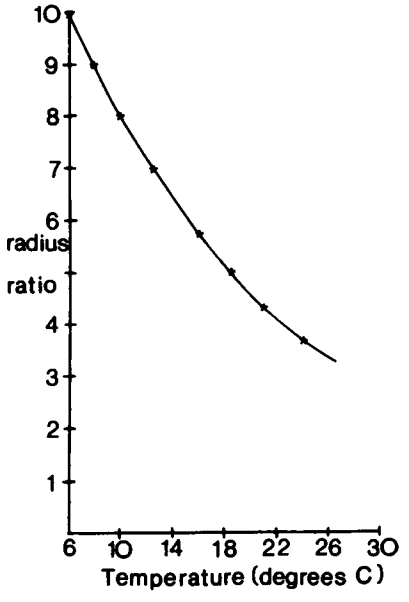

FIGURE 8

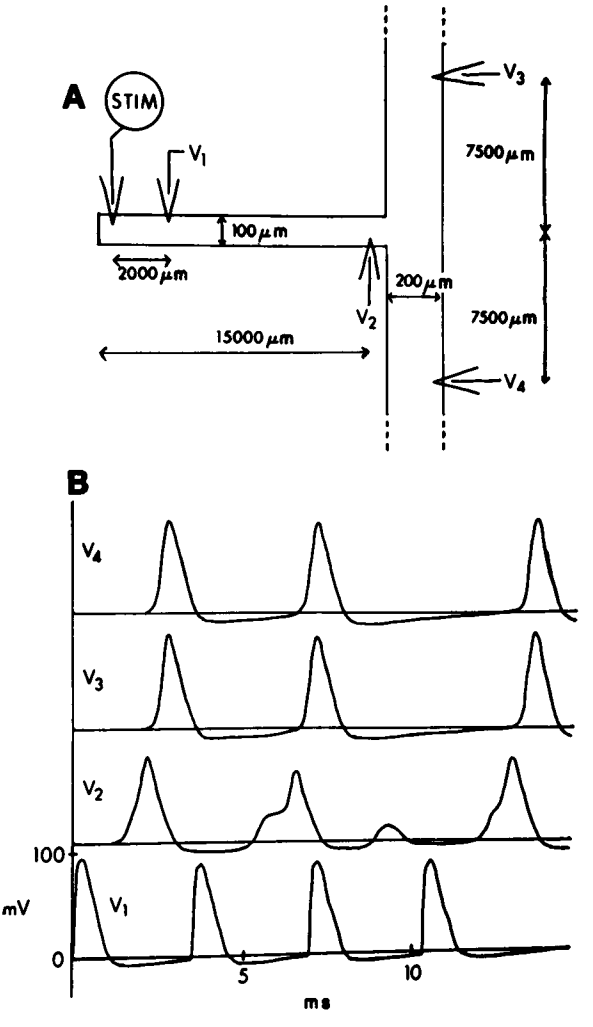

FIGURE 9

FIGURE 8 Effect of temperature on the critical ratio of radii (a_2/a_1) for which propagation will fail at the axon region where the radius abruptly increases from a_1 to a_2.

FIGURE 9 Simulation of a fiber of 200-μm diameter with a branch of 100-μm diameter. Stimulation is at the end of the branch and the four simulated recordings shown in B correspond to the four electrodes shown in A. Stimulus interval was 3.5 ms, temperature 16°C.

single fibers with an abrupt diameter increase. The first action potential in the last segment of the stimulated branch (recording *V*2) shows a slower rate of rise, smaller amplitude, and an increased duration as compared with the action potentials in the uniform regions. The second action potential (stimulated 3.5 ms after the first) shows an even more prominent change in shape, but the third action potential is blocked at the branch point. This failure allows the membrane of the branched region time to

recover excitability. The fourth action potential is able to traverse the branch point almost as easily as the first. This intermittent blocking of impulses is produced by the increased latency and duration of the action potential in the region of the smaller fiber near the branch point, which sees a much larger electrical load than that seen in regions further away from the transition. This increased latency and duration allows the inactivation of the membrane to accumulate so that a high frequency train of impulses will show intermittent failures. A failure allows adequate time for almost complete recovery from inactivation, so that the subsequent spike propagates through the transition region.

It is important to note two factors that restrict the applicability of simulation to propagation failure in real nerve. The first factor is that the Hodgkin-Huxley equations were formulated to describe conductance changes associated with short voltage clamp pulses, and may not adequately describe electrical activity in nerve over long time periods. The second is that these simulations have not taken into account the accumulation of potassium in the extracellular space surrounding the nerve as observed by Frankenhaeuser and Hodgkin (1956). Their experiments and the simulations of membrane action potentials by Adelman and FitzHugh (1975) have shown that potassium accumulation produces marked changes in the response to high frequency trains of stimuli. Nevertheless, it is interesting to know that the Hodgkin-Huxley formulation alone encompasses enough physiological detail to predict intermittent failure at branch points.

DISCUSSION

We have presented here very powerful and general methods that will allow realistic simulations of a complete neuron, including dendritic branches, soma, axon hillock, and axon and terminal arborization. This work extends the compartmental modeling approach used by Rall to simulate a number of geometric properties of passive and excitable cells (Rall, 1964, 1967, 1969, 1970; Rall and Shepherd, 1968). We have initiated investigations of some of these specific regions which will be reported elsewhere (Westerfield et al., 1978; Moore et al., 1978). These studies are being followed by others aimed at giving insight into the interplay of membranes and morphology.

This newly achieved ability to make realistic and detailed computer models of a complete cell emphasizes the need to have detailed descriptions of the membrane and the morphology of each region. If one takes the view that the active membrane properties are not known until each region of the cell has been independently voltage clamped and its properties measured, then we know of no cell that can be realistically modeled. Therefore, membrane properties must be assumed for those regions not yet characterized. We are in a position to model a cell with fully excitable, passive, or a mixture of properties for each region, and to evaluate the effects of these assumptions on the cellular electrical activity.

This lack of detailed data does not pose an immediate problem because there is much to be learned from studies of arbitrarily shaped (or idealized) cells with arbitrarily as-

signed membrane properties. Some examples are reported in this paper. A second application of this method is to investigate the performance of a cell of known geometry using various models and distributions of membrane properties as was done by Dodge and Cooley (1973) for a motoneuron. It may not be possible to assign or distinguish a unique set of membrane properties that fit the behavior of a motoneuron or of any other cells. However, the methods presented here do allow one to independently investigate the contributions of the morphological and membrane characteristics to the electrical behavior of excitable cells.

This work was supported by National Institutes of Health grants NS03437 and NS11613 to J. W. Moore and grant HL19273 to R. W. Joyner.

Received for publication 16 December 1977.

REFERENCES

ADELMAN, W. J., and R. FITZHUGH. 1975. Solutions of the Hodgkin-Huxley equations modified for potassium accumulation in a periaxonal space. *Fed. Proc.* **34**:1322.

CRANK, J., and P. NICHOLSON. 1947. A practical method for numerical evaluation of solutions for partial differential equations of the heat conduction type. *Proc. Cambridge Phil. Soc.* **43**:50.

DODGE, F. A., and J. W. COOLEY. 1973. Action potential of the motoneuron. *IBM J. Res. Develop.* **17**:219.

FRANKENHAEUSER, B., and A. L. HODGKIN. 1956. The after-effects of impulses in the giant nerve fibres of Loligo. *J. Physiol. (Lond.).* **131**:341.

GOLDSTEIN, S., and W. RALL. 1974. Changes of action potential shape and velocity for changing core conductor geometry. *Biophys. J.* **14**:731.

HODGKIN, A. L., and A. F. HUXLEY. 1952. A quantitative description of membrane current and its application to conduction and excitation in nerve. *J. Physiol. (Lond.)* **117**:500.

HUXLEY, A. F. 1959. Ion movements during nerve activity. *Ann. N. Y. Acad. Sci.* **81**:221.

JOYNER, R. W., F. RAMON, and J. W. MOORE. 1975. Simulation of action potential propagation in an inhomogeneous sheet of coupled excitable cells. *Circ. Res.* **36**:654.

KHODOROV, B. I., YE. N. TIMIN, S. YA. VILENKIN, and F. B. GUL'KO. 1969. Theoretical analysis of the mechanism of conduction of a nerve pulse over an inhomogeneous axon. I. Conduction through a portion with increased diameter. *Biophysics* (U.S.S.R.). **14**:304.

KOOTSEY, J. M. 1975. Voltage clamp simulation. *Fed. Proc.* **34**:1342.

LIEBERMAN, M., J. M. KOOTSEY, E. A. JOHNSON, and T. SAWANOBORI. 1973. Slow conduction in cardiac muscle: a biophysical model. *Biophys. J.* **13**:37.

MOORE, J. W., F. RAMON, and R. W. JOYNER. 1975. Axon voltage-clamp simulations. I. Methods and tests. *Biophys. J.* **15**:11.

MOORE, J. W., R. W. JOYNER, M. H. BRILL, S. G. WAXMAN, and M. NAJAR-JOA. 1978. Simulations of conduction in uniform myelinated fibers. *Biophys. J.* **21**:147.

PARNAS, I., S. HOCHSTEIN, and H. PARNAS. 1976. Theoretical analysis of parameters leading to frequency modulation along an inhomogeneous axon. *J. Neurophysiol.* **39**:909.

RALL, W. 1964. Theoretical significance of dendritic trees for neuronal input-output relations. *In* Neural Theory and Modeling. R. F. Reiss, editor. Stanford University Press, Stanford, Calif.

RALL, W. 1967. Distinguishing theoretical synaptic potentials computed for different soma-dendritic distributions of synaptic input. *J. Neurophysiol.* **30**:1138.

RALL, W. 1969. Time constants and electronic length of membrane cylinders and neurons. *Biophys. J.* **9**:1483.

RALL, W. 1970. Cable properties of dendrites and effects of synaptic location. *In* Excitatory Synaptic Mechanisms. P. Anderson and J. K. S. Jansen, editors. Universitets forlaget, Oslo.

RALL, W., and G. M. SHEPHERD. 1968. Theoretical reconstruction of field potentials and dendrodendritic synaptic interactions in olfactory bulb. *J. Neurophysiol.* **31**:884.

RAMON, Fidel, R. W. JOYNER, and J. W. MOORE. 1975. Propagation of action potentials in inhomogeneous axon regions. *Fed. Proc.* **34**:1357.

RAMON, F., J. W. MOORE, R. W. JOYNER, and M. WESTERFIELD. 1976. Squid giant axons: a model for the neuron soma? *Biophys. J.* **16**:953.

WESTERFIELD, N., R. W. JOYNER, and J. W. MOORE. 1978. Temperature-sensitive conduction failure at axon branch points. *J. Neurophysiol.* **41**:1–8.